


Design Anisotropic Broadband ϵ -Near-Zero Metamaterials: Rigorous Use of Bergman and Milton Spectral Representations

Lei Sun,¹ Kin Wah Yu,² and Guo Ping Wang^{1,*}

¹*College of Electronic Science and Technology, Shenzhen University,
3688 Nanhai Boulevard, Shenzhen 518060, People's Republic of China*

²*Department of Physics, The Chinese University of Hong Kong, Shatin, New Territories, Hong Kong*

 (Received 14 January 2017; revised manuscript received 12 March 2018; published 14 June 2018)

A rigorous analytical approach is proposed based on the Bergman spectral representation and the Milton spectral representation of the effective permittivity for a composite system in order to design the anisotropic broadband ϵ -near-zero metamaterials. According to the Bergman and Milton spectral representations, the inverse problem for the anisotropic broadband ϵ -near-zero metamaterials is analytically established and solved by introducing the exactly proved identities. Meanwhile, the introduced identities theoretically reveal the identity of the Bergman and Milton spectral representations in mathematics and physics. With the precise solutions to the inverse problem, the conditions for designing the anisotropic broadband ϵ -near-zero metamaterials are clarified and demonstrated by the specific anisotropic broadband ϵ -near-zero meta-atoms of the lamination and the Hashin-Shtrikman coated-sphere microstructures through a theoretical analysis and a computational full-wave simulation.

DOI: [10.1103/PhysRevApplied.9.064020](https://doi.org/10.1103/PhysRevApplied.9.064020)

I. INTRODUCTION

Metamaterials, artificially structured materials with sub-wavelength components, have come into focus during explorations in both fundamental scientific research and engineering applications in recent decades because of their extraordinary macroscopic electromagnetic properties, which do not exist in nature [1–13]. Among all kinds of metamaterials, the ones with near-zero permittivity [ϵ near zero (ENZ)], coming into view due to their unique electromagnetic features, are of great importance in many applications at microwave and optical frequencies [14–29]. In fact, it is possible to obtain ENZ metamaterials at a single operating frequency. However, regarding the practical implementations, ENZ metamaterials over a broadband operating frequency range are required, which is a challenge in both science and technology. Concerning this problem, a straightforward solution is similar to a brute-force attack made by optimizing an objective function mapping the effective permittivity onto the component properties of the ENZ metamaterials [30–34]. In principle, the objective-function-optimization approach is straightforward, but it is cumbersome for practical applications. Theoretically, the broadband ENZ metamaterials design is just an inverse problem of effective-medium theory (EMT) [35]. On these grounds, the authors suggest an efficient approach [36–40] by numerically solving the EMT

inverse problem based on the spectral representations that were established by Bergman [41,42] and Milton [43–46] and mathematically elaborated on by Golden and Papanicolaou [47] for the effective permittivity. Although it reveals the tip of the iceberg, the approach is still very insufficient because it only numerically solves the problem without analytically clarifying the physical and mathematical fundamentals.

In regard to the insufficiency, a type of anisotropic broadband metal-dielectric ENZ metamaterials of the lamination and the Hashin-Shtrikman coated-sphere microstructures [48] is designed according to the Bergman and Milton spectral representations by rigorously solving the EMT inverse problem analytically. During the design progress, the existence and the stability of the EMT inverse problem are fully discussed based on the exactly proved identities, while the identities of the Bergman and Milton spectral representation are also revealed. Furthermore, the full-wave simulation based on the finite-element method (FEM) numerically confirms the correctness of the theoretical design. For convenience, this work is organized as follows. Section II provides analytical studies about the EMT inverse problem for the broadband ENZ metamaterials, and the general solutions to the inverse problem are obtained. Section III provides a specific solution to the inverse problem which indicates a practicable method to design broadband ENZ metamaterials, and it demonstrates an exact example with respect to the specific solution of the inverse problem. Finally, Sec. IV provides a full-wave simulation about the theoretically designed anisotropic

*Corresponding author.
gpwang@szu.edu.cn

broadband ENZ metamaterials, which verifies the correctness of the design. It is worth mentioning that all important derivations in this work are thoroughly discussed in the Supplemental Material [49].

II. THE INVERSE PROBLEM FOR THE BROADBAND ENZ METAMATERIALS

Anisotropic broadband ENZ metamaterials are periodically constructed with identical broadband ENZ meta-atoms (unit cells) schematically displayed in Fig. 1 as an N -layer stack. In general, the meta-atom is a two-phase (of permittivities ε_1 and ε_2 , respectively) composite system with scales less than the wavelength of the electromagnetic wave in the operating frequency range. The two components in each layer take the Hashin-Shtrikman coated-sphere microstructure. The thickness of each layer d_i is normalized by the thickness of the meta-atom, which implies that $0 < d_i < 1$ and $\sum_{i=1}^N d_i \equiv 1$ (the thickness summation rule). The volume fractions of the two components in each layer are denoted as $f_1^{(i)}$ and $f_2^{(i)}$, with the conditions $0 < f_1^{(i)}, f_2^{(i)} < 1$, and $f_1^{(i)} + f_2^{(i)} \equiv 1$. The structures of the meta-atom are chosen based on the fact that the effective permittivities for the Hashin-Shtrikman coated-sphere microstructure and the N -layer stack can be exactly obtained. According to the Maxwell-Garnett approximation [50,51], the effective permittivity of each layer reads

$$\frac{\varepsilon_e^{(i)} - \varepsilon_1}{\varepsilon_e^{(i)} + 2\varepsilon_1} = (1 - f_1^{(i)}) \frac{\varepsilon_2 - \varepsilon_1}{\varepsilon_2 + 2\varepsilon_1}. \quad (1)$$

By introducing the s parameter $s = \varepsilon_2/(\varepsilon_2 - \varepsilon_1)$, Eq. (1) can be rewritten as

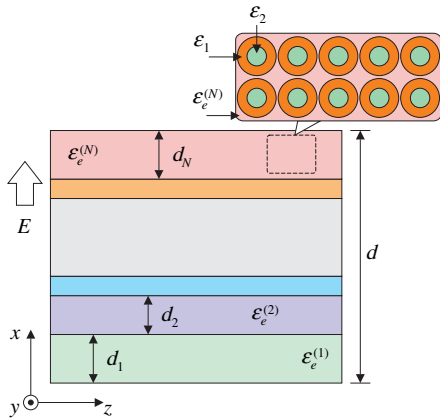


FIG. 1. Schematic of the meta-atom of the broadband ENZ metamaterials with the lamination and the Hashin-Shtrikman coated-sphere microstructures.

$$\varepsilon_e^{(i)} = \varepsilon_2 \frac{s-1}{s} \frac{s-2f_1^{(i)}/3}{s-(3-f_1^{(i)})/3} \quad (2)$$

in terms of the Milton spectral representation format [49]. In addition, the effective permittivity of the meta-atom can be determined as

$$\varepsilon_e = \left[\sum_{i=1}^N \frac{d_i}{\varepsilon_e^{(i)}} \right]^{-1}, \quad (3)$$

which can be expressed as

$$\frac{\varepsilon_2}{\varepsilon_e} = \frac{s}{s-1} \left[1 - \sum_{i=1}^N \frac{(1-f_1^{(i)})d_i}{s-2f_1^{(i)}/3} \right], \quad (4)$$

according to Eq. (2) and the thickness summation rule. Alternatively, the effective permittivity of the meta-atom can be directly obtain based on the Milton spectral representation as

$$\frac{\varepsilon_2}{\varepsilon_e} = \frac{s}{s-1} \prod_{i=1}^N \frac{s-s'_i}{s-z'_i} = \frac{s}{s-1} \left[1 - \sum_{i=1}^N \frac{\prod_{j=1}^N (s'_j - z'_i)}{(s-z'_i) \prod_{j \neq i}^N (z'_j - z'_i)} \right], \quad (5)$$

which implies the identity between the Milton spectral representation and the Bergman spectral representation [49]. Note that, because of the constant pole $s^* \equiv 0$ and the constant zero $z^* \equiv 1$ in Eq. (2), the pole-zero series rule for Eq. (5) should be modified as

$$s^* \equiv 0 < z'_1 < s'_1 < \dots < z'_i < s'_i < \dots < z'_N < s'_N < z^* \equiv 1, \quad (6)$$

in accordance with the request of the Milton spectral representation.

For the same meta-atom, Eqs. (4) and (5) must provide the same results; thus, the inverse problem is set up as

$$\sum_{i=1}^N \frac{(1-f_1^{(i)})d_i}{s-2f_1^{(i)}/3} = \sum_{i=1}^N \frac{\prod_{j=1}^N (s'_j - z'_i)}{(s-z'_i) \prod_{j \neq i}^N (z'_j - z'_i)}, \quad (7)$$

and the corresponding solutions can be straightforwardly obtained as

$$f_1^{(i)} = 3z'_i/2, \quad (8)$$

$$d_i = \frac{\prod_{j=1}^N (s'_j - z'_i)}{(1-3z'_i/2) \prod_{j \neq i}^N (z'_j - z'_i)}, \quad (9)$$

with the confinement of

$$0 < z'_i < 2/3, \quad (10)$$

$$\prod_{i=1}^N \frac{1 - 3s'_i/2}{1 - 3z'_i/2} \equiv -\frac{1}{2}, \quad (11)$$

according to the physical restrictions of the thicknesses and the volume fractions [49].

III. THE SPECIFIC ANISOTROPIC METAL-DIELECTRIC BROADBAND ENZ META-ATOMS

According to the solution, the design of the meta-atoms of the anisotropic broadband ENZ metamaterials is flexible. For instance, an N -layered broadband ENZ meta-atom can be constructed, based on the following pole-zero series, as

$$z'_i = z'_1 + (i-1)\Delta \quad (0 < z'_i < 2/3 \text{ and } i = 1, 2, 3, \dots, N), \quad (12)$$

$$s'_i = \begin{cases} z'_i + (\varrho - 1)(2 - 3z'_i)/(3\varrho) & (i = 1, 2, 3, \dots, N-1) \\ 2/3 + \rho(2 - 3z'_N)/3 & (i = N) \end{cases}, \quad (13)$$

with the parameter $\Delta = (z'_N - z'_1)/(N-1)$ and the parameter $\varrho = \sqrt[N]{2\rho}$, under the confinement of

$$\frac{1}{2} = \rho_{\min} < \rho < \rho_{\max} = \frac{1}{2} \left[1 + \frac{3\Delta}{(2 - 3z'_1) - 3\Delta} \right]^{N-1}. \quad (14)$$

A detailed analysis of the specific design above is shown in the Supplemental Material [49].

As an exact example, consider the broadband ENZ meta-atom composed of the noble metal Au (gold) as the host component (ε_1) and the dielectric material SiO₂ (fused silica) as the inclusion (ε_2). For mathematical convenience, the permittivity of Au is described by the Drude model as

$$\varepsilon_1(\omega) = \varepsilon_\infty - \frac{\omega_p^2}{\omega(\omega + \mathbf{i}\gamma)}, \quad (15)$$

with the offset constant $\varepsilon_\infty = 9$, the plasma frequency $\omega_p = 13.8 \times 10^{15}$ rad/s, and the damping constant $\gamma = 0.11 \times 10^{15}$ rad/s [52]. The Drude model in Eq. (15) shows good agreement with the experimental result of Ref. [53] in the frequency range from approximately $0.07\omega_p$ (154.772 THz) to $0.273\omega_p$ (600.0 THz). Meanwhile, the permittivity of SiO₂ is set at $\varepsilon_2 = 1.45^2$ according to the experimental results of Ref. [54].

TABLE II. Values of thicknesses and volume fractions in the lossless case.

	$i = 1$	$i = 2$	$i = 3$	$i = 4$
d_i	0.314 017	0.182 546	0.183 647	0.319 790
$f_1^{(i)}$	0.033 874	0.050 580 9	0.067 287 9	0.083 994 9

For the sake of convenience, the lossless case (the material loss of Au is ignored) is explored at first. In such a case, according to the Milton spectral representation in Eq. (5) and the pole-zero series rule in Eq. (6), it is clear that the possible operating frequency range for the broadband ENZ meta-atoms is confined in the frequency range, where the s parameter is confined as $0 < s < 1$. In other words, the operating frequency range is determined by the permittivities of the two individual components since the s parameter is directly related to the components' permittivities. With respect to the permittivity of Au and the permittivity of SiO₂, it is found that the possible operating frequency range lies in the whole frequency range, where the Drude model in Eq. (15) works properly. Without loss of generality, the operating frequency range is set at $0.1\omega_p$ (219.634 THz) to $0.15\omega_p$ (329.451 THz), while the number of layers in one meta-atom is set at $N = 4$. Correspondingly, the zero series can be determined by Eq. (12), with $z'_1 = s(0.1\omega_p)$ and $z'_{N=4} = s(0.15\omega_p)$ based on the dimensional analysis about the Milton spectral representation, while the related poles series can be determined via Eq. (13). Table I lists all values of the pole-zero series. It is clear that the pole-zero series list in Table I satisfies the pole-zero series rule in Eq. (6). Associated with the above pole-zero series, the thicknesses and the volume fractions read as Table II based on Eqs. (8) and (9). Note that the thickness summation rule is satisfied. Regarding the effective permittivity, Fig. 2(a) displays the variation of the effective permittivity as a function of the s parameter based on the Milton spectral representation. It is obvious that, without material loss, the effective permittivity reaches a zero value when the s parameter meets all zeros, and it extends to infinity when the s parameter approaches all poles, which coincides with the prediction of the Milton spectral representation. Similar variations of the effective permittivity can also be observed when the s parameter is mapped onto frequency space, as depicted in Fig. 2(b).

Regarding the case in which the material loss is taken into account, the s parameter is a complex function with respect to the frequency. Therefore, the possible operating

TABLE I. Values of the pole-zero series in the lossless case.

		$i = 1$	$i = 2$	$i = 3$	$i = 4$	
s'_i	$s^* \equiv 0$	0.028 248 8	0.039 288 8	0.050 327 8	0.980 204	
z'_i		0.022 582 6	0.033 720 6	0.044 858 6	0.055 996 6	$z^* \equiv 1$

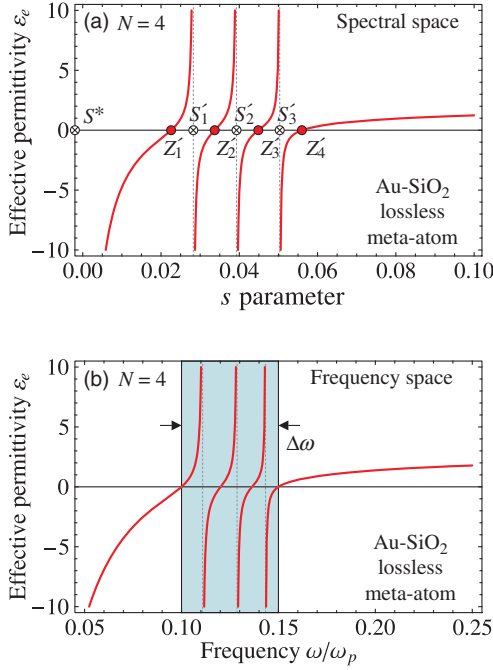


FIG. 2. The effective permittivity of the $N = 4$ layer Au-SiO₂ broadband ENZ meta-atom without material loss in (a) the spectral space with the poles marked as crosses with circles and the zeros marked as solid dots, and (b) the corresponding frequency space with the operating frequency range $\Delta\omega$ of $0.1\omega_p$ to $0.15\omega_p$.

frequency range may lie in the confined frequency range, where $0 < \text{Re}(s) < 1$. Meanwhile, the boundaries of the pole-zero series can be determined with $z'_1 = \text{Re}[s(0.1\omega_p)]$ and $z'_{N=4} = \text{Re}[s(0.15\omega_p)]$, as listed in Table III with respect to a meta-atom design similar to the one discussed above. Repeating the same procedure, the microstructures of the meta-atom can be obtained as in Table IV. Associated with the thicknesses and the volume fractions in Table IV, the corresponding effective permittivity is displayed in Fig. 3(a). Clearly, the real part of the effective permittivity oscillates around the value of zero with a small fluctuation in the operating frequency range, and it leads to a vibration of the imaginary part of the effective permittivity due to the Kramers-Kronig relations [55–57]. Further calculations indicate that the mean value of the real part of the effective permittivity is about $\langle \text{Re}(\varepsilon_e) \rangle = \int \text{Re}(\varepsilon_e) \omega d\omega / \Delta\omega = 0.0127669$ in the operating frequency range. It is worth noting that, due to the material loss, the real part of the effective permittivity will not be exactly zero at all zeros,

TABLE IV. Values of thicknesses and volume fractions in the lossy case.

	$i = 1$	$i = 2$	$i = 3$	$i = 4$
d_i	0.314 016	0.182 549	0.183 649	0.319 786
$f_1^{(i)}$	0.033 856 8	0.050 552 3	0.067 247 8	0.083 943 3

while the oscillation may not always be around the zero value with respect to the increase of the frequency, as marked by the arrow in Fig. 3(a). In previous studies, the zero-variation method is numerically proposed to improve the quality of the results [37]. However, unlike previous studies, the pole-zero series are strongly tangled through Eq. (11); thus, the zero-variation method cannot be applied here. With respect to this problem, the iteration method is proposed and performed as follows. First, according to the obtained pole-zero series (e.g., the pole-zero series in Table III), solve the equation $\text{Re}[\varepsilon_e(s'_i, z''_i)] = 0$ with all poles being fixed, which produces a new zero series denoted as z''_i . Second, according to the new zero series z''_i and Eq. (13), a new pole series denoted as s''_i can be obtained. Finally, the new pole-zero series can yield revised thicknesses and revised volume fractions based on Eqs. (8) and (9). Figure 3(b) shows the effective permittivity obtained from the iterative method, which makes it clear that the deviation in Fig. 3(a) is amended (marked by the arrow). Correspondingly, the mean value of the real part of the effective permittivity is about $\langle \text{Re}(\varepsilon_e) \rangle = 0.0071841$, which is almost half of the previous result.

Besides the iteration method, there are also other efficient approaches to reduce the fluctuation of the effective permittivity. For example, a moderate increase in the layer number of the meta-atom can efficiently reduce the fluctuation. Figure 4(a) demonstrates the effective permittivity of the broadband ENZ meta-atom with $N = 6$ layers in the same operating frequency range studied previously. Obviously, the fluctuation in the effective permittivity is notably reduced, and the mean value of the real part of the effective permittivity decreases to about $\langle \text{Re}(\varepsilon_e) \rangle = -3.9 \times 10^{-4}$. In addition, since the permittivities of the individual components in the broadband ENZ meta-atom are the key points in the design of the broadband ENZ meta-atom, a proper choice on the components can also improve the quality of the broadband ENZ meta-atom. As an example, Fig. 4(b) shows the effective permittivity of the broadband ENZ meta-atom composed with Au and air (permittivity $\varepsilon_2 = 1$), e.g., metal host with microscale air

TABLE III. Values of the pole-zero series in the lossy case.

		$i = 1$	$i = 2$	$i = 3$	$i = 4$	
s'_i	$s^* \equiv 0$	0.028 233 4	0.039 265 9	0.050 298 3	0.980 216	
z'_i		0.022 571 2	0.033 701 5	0.044 831 9	0.055 962 2	$z^* \equiv 1$

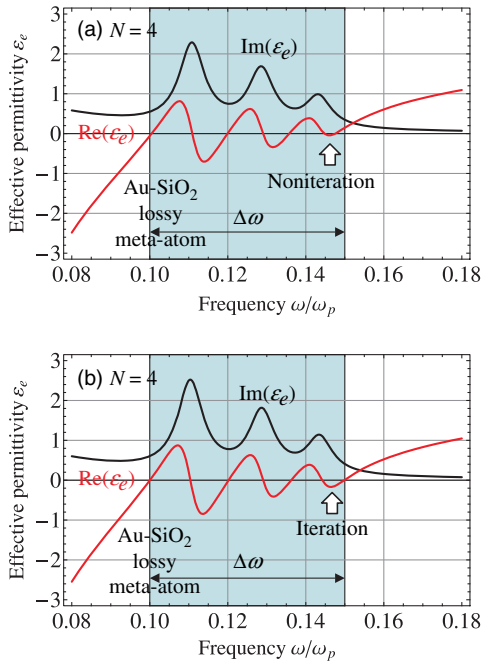


FIG. 3. The effective permittivity of the $N = 4$ layer Au-SiO₂ broadband ENZ meta-atom with material loss in the operating frequency range $\Delta\omega$ of $0.1\omega_p$ to $0.15\omega_p$ determined by the inverse problem (a) without the iteration modification and (b) with the iteration modification, respectively.

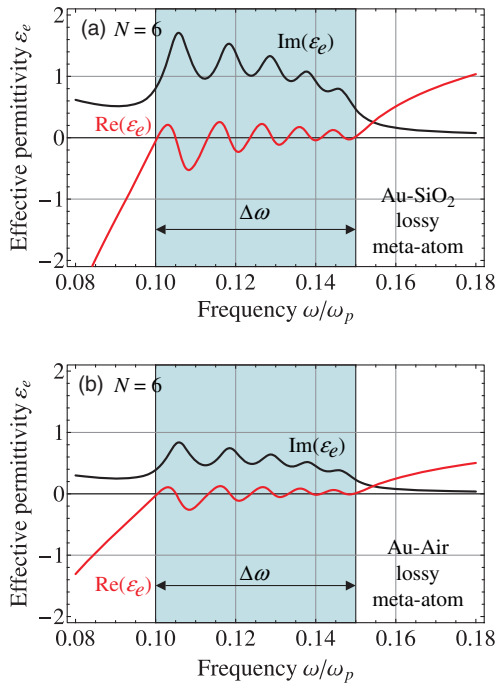


FIG. 4. The effective permittivity of the $N = 6$ layer (a) Au-SiO₂ broadband ENZ meta-atom and (b) Au-air broadband ENZ meta-atom with material loss in the operating frequency range $\Delta\omega$ of $0.1\omega_p$ to $0.15\omega_p$.

bubbles as inclusions, with the number of layers $N = 6$ and the same operating frequency range as previously used. It is clear that by reducing the permittivity of the dielectric component in the meta-atom, the fluctuation in the effective permittivity can be significantly reduced, and the calculation result indicates that the mean value of the real part of the effective permittivity of the Au-air broadband ENZ meta-atom is about $\langle \text{Re}(\epsilon_e) \rangle = -7.4 \times 10^{-5}$, i.e., almost 1 order fewer than the Au-SiO₂ broadband ENZ meta-atom.

IV. FULL-WAVE SIMULATION

The Bergman and Milton spectral representations of the effective permittivity are under the quasistatic approximation, which implies that the theoretical design procedure discussed above is also limited in the long-wavelength condition. Regarding the practical applications, the full-wave condition must be taken into account. Therefore, a FEM computational full-wave simulation is performed with respect to the specific broadband ENZ meta-atom, and the results are displayed in Fig. 5.

As depicted in Fig. 5(a), the simulation model is carried out in three-dimensional space with an $N = 4$ layer broadband ENZ meta-atom sandwiched between two identical layers of air. A plane electromagnetic wave of the electric field E_x is stimulated at the bottom (port 1) of the model and received at the top (port 2). Besides, all other outer surfaces of the model are regarded as periodic boundaries. The broadband ENZ meta-atom is of the fixed length $d_z = 50$ nm, but it has a variable cross section $d_x \times d_y$. For comparison, two different cross sections are considered, i.e., 20×10 nm (case I) and 40×20 nm (case II). As in Fig. 1, the layers of the broadband ENZ meta-atom are arranged along the x direction with the thickness and the volume fraction given in Table IV. Furthermore, the outer diameter of the Au-SiO₂ Hashin-Shtrikman coated-sphere particle is set at $(3/4)d_i$ for each layer. In general, the simulation directly calculates the complex scattering parameters S_{11} and S_{21} , which are related to the reflection coefficient and the transmission coefficient of the broadband ENZ meta-atom, respectively, including the distribution of the electric field and the electric displacement field in the broadband ENZ meta-atom. Regarding the complex scattering parameter, Figs. 5(b) and 5(c) individually demonstrate the absolute values and the arguments (in terms of the principal values) for the broadband ENZ meta-atom with the two different cross sections. It is obvious that both the absolute values and the arguments of the complex scattering parameters possess a particular oscillation in the designed operating frequency range of the broadband ENZ meta-atom, which implies the broadband ENZ properties.

On the other hand, the effective permittivities of the broadband ENZ meta-atom can be retrieved from the simulated complex scattering parameters according to the retrieved algorithm [58], as illustrated in Figs. 5(d) and 5(e) by solid curves. It is clear that the retrieved

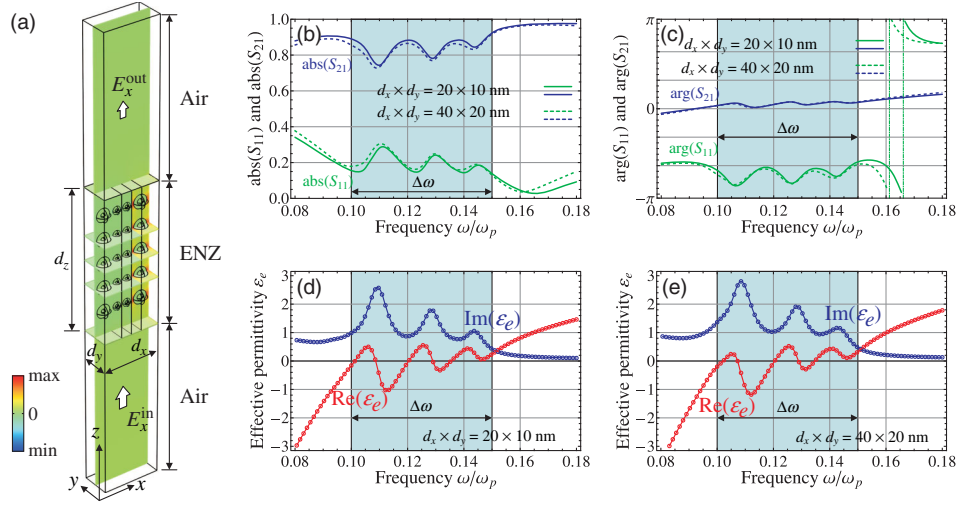


FIG. 5. (a) The three-dimensional full-wave simulation model of the $N = 4$ layer Au-SiO₂ broadband ENZ meta-atom with the fixed length $d_z = 50$ nm and the variable cross sections $d_x \times d_y$. An x -polarized plane electromagnetic wave is stimulated at the bottom and received at the top. All other outer surfaces of the model are set to be periodic. (b) The absolutely values and (c) the arguments in principal values of the complex scattering parameters are displayed in solid curves for a meta-atom with a cross section of 20×10 nm, and in dashed curves for a meta-atom with a cross section of 40×20 nm. The retrieved effective permittivities based on the complex scattering parameters (the solid curves) and the definition (the circles) of the meta-atom are indicated, respectively, for (d) the (20×10) -nm cross section and (e) the (40×20) -nm cross section.

effective permittivities possess a broadband ENZ properties in the designed operating frequency range, which coincides with the theoretical prediction [Fig. 3(a)]. However, it is still worth stressing that, although the broadband ENZ meta-atom is of the subwavelength size, the optical nonlocality in the meta-atom in the full-wave condition cannot be fully neglected. Especially when the size of the broadband ENZ meta-atom increases, the inevitable optical nonlocality leads to more fluctuations in the effective permittivity compared with the theoretical prediction, which can be observed from the result in Fig. 5(e). Furthermore, besides the scattering-parameter-retrieval algorithm, the effective permittivity can also be obtained according to the definition $\epsilon_e = \langle D_x \rangle / \langle E_x \rangle$, in which the mean value of the electric displacement field and the electric field can both be achieved from the simulation directly. For comparison, the effective permittivities based on the definition are also displayed in Figs. 5(d) and 5(e), as circles. Clearly, both methods show the same results for the effective permittivities. Therefore, we have evidence that the theoretical design procedure is accurate with respect to the practical applications in the full-wave condition.

Finally, the computational full-wave simulation also reveals the physics behind the anisotropic broadband ENZ metamaterial design. Generally, the broadband ENZ meta-atom can be regarded as a coupled waveguide system. Each layer of the broadband ENZ meta-atom can be considered as a single waveguide of the ENZ property at a single operating frequency, while the ENZ frequency is

determined by the properties of the components according to the Maxwell-Garnett approximation. Meanwhile, the thickness of each layer, which is obtained through the EMT inverse problem, tunes only the coupling strength between each layer. Therefore, the whole meta-atom, working as a well-tuned coupled waveguide system, performs the broadband ENZ properties.

V. CONCLUSIONS

To conclude, based on the compact format of the Milton spectral representation, the rigorous analytical solutions to the EMT inverse problem regarding the design of the anisotropic broadband ENZ metamaterials is obtained by introducing the exactly proved identities. According to the analytical solutions, the anisotropic broadband metal-dielectric ENZ metamaterials of the lamination and the Hashin-Shtrikman coated-sphere microstructures is designed and demonstrated through theoretical analysis and full-wave simulation. In addition, the existence and the stability of the solutions to the inverse problem are studied in detail. Furthermore, regarding practical applications, improvements in design strategy are also suggested, including the iteration method on the microstructure modification and the choice of the individual component materials. Finally, it is worth stressing that the method discussed above indicates an inevitable high imaginary part in the effective permittivity over the designed operating frequency range. Therefore, there is still a long way to go to achieve the ideal broadband ENZ response.

ACKNOWLEDGMENTS

This work was supported by the National Science Foundation of Shenzhen University (Grant No. 2017006) and the National Natural Science Foundation of China (NSFC) (Grants No. 11574218 and No. 11734012).

-
- [1] V.G. Veselago, The electrodynamics of substances with simultaneously negative values of ϵ and μ , *Sov. Phys. Usp.* **10**, 509 (1968).
- [2] D.R. Smith, J.B. Pendry, and M.C.K. Wiltshire, Metamaterials and negative refractive index, *Science* **305**, 788 (2004).
- [3] J.B. Pendry, D. Schurig, and D.R. Smith, Controlling electromagnetic fields, *Science* **312**, 1780 (2006).
- [4] K.L. Tsakmakidis, A.D. Boardman, and O. Hess, “Trapped rainbow” storage of light in metamaterials, *Nature (London)* **450**, 397 (2007).
- [5] J. Valentine, S. Zhang, T. Zentgraf, E. Ulin-Avila, D.A. Genov, G. Bartal, and X. Zhang, Three-dimensional optical metamaterial with a negative refractive index, *Nature (London)* **455**, 376 (2008).
- [6] T. Driscoll, H.-T. Kim, B.-G. Chae, B.-J. Kim, Y.-W. Lee, N. M. Jokerst, S. Palit, D. R. Smith, M. Di Ventra, and D. N. Basov, Memory metamaterials, *Science* **325**, 1518 (2009).
- [7] S. Xiao, V.P. Drachev, A.V. Kildishev, X. Ni, U.K. Chettiar, H.-K. Yuan, and V.M. Shalaev, Loss-free and active optical negative-index metamaterials, *Nature (London)* **466**, 735 (2010).
- [8] A. Boltasseva and H. A. Atwater, Low-loss plasmonic metamaterials, *Science* **331**, 290 (2011).
- [9] H.N.S. Krishnamoorthy, Z. Jacob, E. Narimanov, I. Kretzschmar, and V.M. Menon, Topological transitions in metamaterials, *Science* **336**, 205 (2012).
- [10] A. Poddubny, I. Iorsh, P. Belov, and Y. Kivshar, Hyperbolic metamaterials, *Nat. Photonics* **7**, 948 (2013).
- [11] A. Silva, F. Monticone, G. Castaldi, V. Galdi, A. Alù, and N. Engheta, Performing mathematical operations with metamaterials, *Science* **343**, 160 (2014).
- [12] J. Paulose, B. Gin-ge Chen, and V. Vitelli, Topological modes bound to dislocations in mechanical metamaterials, *Nat. Phys.* **11**, 153 (2015).
- [13] S. Jahani and Z. Jacob, All-dielectric metamaterials, *Nat. Nanotechnol.* **11**, 23 (2016).
- [14] M. Silveirinha and N. Engheta, Tunneling of Electromagnetic Energy through Subwavelength Channels and Bends Using ϵ -Near-Zero Materials, *Phys. Rev. Lett.* **97**, 157403 (2006).
- [15] A. Alù, M. G. Silveirinha, A. Salandrino, and N. Engheta, Epsilon-near-zero metamaterials and electromagnetic sources: Tailoring the radiation phase pattern, *Phys. Rev. B* **75**, 155410 (2007).
- [16] M. Silveirinha and N. Engheta, Design of matched zero-index metamaterials using nonmagnetic inclusions in epsilon-near-zero media, *Phys. Rev. B* **75**, 075119 (2007).
- [17] R. Liu, Q. Cheng, T. Hand, J.J. Mock, T.J. Cui, S. A. Cummer, and D. R. Smith, Experimental Demonstration of Electromagnetic Tunneling through an Epsilon-Near-Zero Metamaterial at Microwave Frequencies, *Phys. Rev. Lett.* **100**, 023903 (2008).
- [18] B. Edwards, A. Alù, M.E. Young, M. Silveirinha, and N. Engheta, Experimental Verification of Epsilon-Near-Zero Metamaterial Coupling and Energy Squeezing Using a Microwave Waveguide, *Phys. Rev. Lett.* **100**, 033903 (2008).
- [19] R. J. Pollard, A. Murphy, W.R. Hendren, P.R. Evans, R. Atkinson, G. A. Wurtz, A. V. Zayats, and V. A. Podolskiy, Optical Nonlocalities and Additional Waves in Epsilon-Near-Zero Metamaterials, *Phys. Rev. Lett.* **102**, 127405 (2009).
- [20] D. C. Adams, S. Inampudi, T. Ribaldo, D. Slocum, S. Vangala, N. A. Kuhta, W. D. Goodhue, V. A. Podolskiy, and D. Wasserman, Funneling Light through a Subwavelength Aperture with Epsilon-Near-Zero Materials, *Phys. Rev. Lett.* **107**, 133901 (2011).
- [21] S. Vassant, A. Archambault, F. Marquier, F. Pardo, U. Gennser, A. Cavanna, J.L. Pelouard, and J.J. Greffet, Epsilon-Near-Zero Mode for Active Optoelectronic Devices, *Phys. Rev. Lett.* **109**, 237401 (2012).
- [22] S. Feng and K. Halterman, Coherent perfect absorption in epsilon-near-zero metamaterials, *Phys. Rev. B* **86**, 165103 (2012).
- [23] R. Maas, J. Parsons, N. Engheta, and A. Polman, Experimental realization of an epsilon-near-zero metamaterial at visible wavelengths, *Nat. Photonics* **7**, 907 (2013).
- [24] S. Savoia, G. Castaldi, V. Galdi, A. Alù, and N. Engheta, Tunneling of obliquely incident waves through \mathcal{PT} -symmetric epsilon-near-zero bilayers, *Phys. Rev. B* **89**, 085105 (2014).
- [25] C. Rizza, A. Di Falco, M. Scalora, and A. Ciattoni, One-Dimensional Chirality: Strong Optical Activity in Epsilon-Near-Zero Metamaterials, *Phys. Rev. Lett.* **115**, 057401 (2015).
- [26] Y. Xu, C. T. Chan, and H. Chen, Goos-Hänchen effect in epsilon-near-zero metamaterials, *Sci. Rep.* **5**, 8681 (2015).
- [27] M. Lobet, B. Majerus, L. Henrard, and P. Lambin, Perfect electromagnetic absorption using graphene and epsilon-near-zero metamaterials, *Phys. Rev. B* **93**, 235424 (2016).
- [28] M.H. Javani and M.I. Stockman, Real and Imaginary Properties of Epsilon-Near-Zero Materials, *Phys. Rev. Lett.* **117**, 107404 (2016).
- [29] A. Ciattoni, C. Rizza, A. Marini, A. Di Falco, D. Faccio, and M. Scalora, Enhanced nonlinear effects in pulse propagation through epsilon-near-zero media, *Laser Photonics Rev.* **10**, 517 (2016).
- [30] A. V. Goncharenko and K.-R. Chen, Strategy for designing epsilon-near-zero nanostructured metamaterials over a frequency range, *J. Nanophoton.* **4**, 041530 (2010).
- [31] A. V. Goncharenko and K.-R. Chen, Errata: Strategy for designing epsilon-near-zero nanostructured metamaterials over a frequency range, *J. Nanophoton.* **4**, 040101 (2010).
- [32] A. V. Goncharenko, V. U. Nazarov, and K.-R. Chen, Development of metamaterials with desired broadband optical properties, *Appl. Phys. Lett.* **101**, 071907 (2012).
- [33] A. V. Goncharenko, V. U. Nazarov, and K.-R. Chen, Nanostructured metamaterials with broadband optical properties, *Opt. Mater. Express* **3**, 143 (2013).

- [34] A. V. Goncharenko, E. F. Venger, Y. C. Chang, and A. O. Pinchuk, Arrays of core-shell nanospheres as 3D isotropic broadband ENZ and highly absorbing metamaterials, *Opt. Mater. Express* **4**, 2310 (2014).
- [35] T. C. Choy, *Effective Medium Theory: Principles and Applications* (Oxford University Press, Oxford, 2015).
- [36] L. Sun and K. W. Yu, Strategy for designing broadband epsilon-near-zero metamaterials, *J. Opt. Soc. Am. B* **29**, 984 (2012).
- [37] L. Sun and K. W. Yu, Strategy for designing broadband epsilon-near-zero metamaterial with loss compensation by gain media, *Appl. Phys. Lett.* **100**, 261903 (2012).
- [38] L. Sun, K. W. Yu, and X. Yang, Integrated optical devices based on broadband epsilon-near-zero meta-atoms, *Opt. Lett.* **37**, 3096 (2012).
- [39] L. Sun, J. Gao, and X. Yang, Broadband epsilon-near-zero metamaterials with steplike metal-dielectric multilayer structures, *Phys. Rev. B* **87**, 165134 (2013).
- [40] L. Sun, X. Yang, and J. Gao, Loss-compensated broadband epsilon-near-zero metamaterials with gain media, *Appl. Phys. Lett.* **103**, 201109 (2013).
- [41] D. J. Bergman, The dielectric constant of a composite material—A problem in classical physics, *Phys. Rep.* **43**, 377 (1978).
- [42] D. J. Bergman and D. Stroud, Physical properties of macroscopically inhomogeneous media, *Solid State Phys.* **46**, 147 (1992).
- [43] G. W. Milton, Bounds on the complex dielectric constant of a composite material, *Appl. Phys. Lett.* **37**, 300 (1980).
- [44] G. W. Milton, Bounds on the complex permittivity of a two-component composite material, *Appl. Phys. Lett.* **52**, 5286 (1981).
- [45] G. W. Milton, Bounds on the transport and optical properties of a two-component composite materials, *Appl. Phys. Lett.* **52**, 5294 (1981).
- [46] G. W. Milton, *The Theory of Composites* (Cambridge University Press, Cambridge, England, 2002).
- [47] K. Golden and G. Papanicolaou, Bounds for effective parameters of heterogeneous media by analytic continuation, *Commun. Math. Phys.* **90**, 473 (1983).
- [48] Z. Hashin and S. Shtrikman, A variational approach to the elastic behavior of multiphase minerals, *J. Mech. Phys. Solids* **11**, 127 (1963).
- [49] See Supplemental Material at <http://link.aps.org/supplemental/10.1103/PhysRevApplied.9.064020> for the detailed derivations.
- [50] J. C. M. Garnett, Colours in metal glasses and in metallic films, *Phil. Trans. R. Soc. A* **203**, 385 (1904).
- [51] J. C. M. Garnett, Colours in metal glasses, in metallic films, and in metallic solutions. II, *Phil. Trans. R. Soc. A* **205**, 237 (1906).
- [52] W. Cai and V. Shalaev, *Optical Metamaterials: Fundamentals and Applications* (Springer, Berlin, 2010).
- [53] P. B. Johnson and R. W. Christy, Optical constants of noble metals, *Phys. Rev. B* **6**, 4370 (1972).
- [54] I. H. Malitson, Interspecimen comparison of the refractive index of fused silica, *J. Opt. Soc. Am.* **55**, 1205 (1965).
- [55] R. de L. Kronig, On the theory of the dispersion of x-rays, *J. Opt. Soc. Am.* **12**, 547 (1926).
- [56] H. A. Kramers, The diffusion of light by atoms, *Atti Cong. Intern. Fisica (Trans. Volta Centenary Congr.) Como.* **2**, 545 (1927).
- [57] J. S. Toll, Causality and the dispersion relation: Logical foundations, *Phys. Rev.* **104**, 1760 (1956).
- [58] X. Chen, T. M. Grzegorzczuk, B.-I. Wu, J. Pacheco, Jr., and J. A. Kong, Robust method to retrieve the constitutive effective parameters of metamaterials, *Phys. Rev. E* **70**, 016608 (2004).